TOPICS AND INSTRUMENTATION IN CHEMICAL REACTION DYNAMICS

A Dissertation

Presented to the Faculty of the Graduate School

of Cornell University

In Partial Fulfillment of the Requirements for the Degree of

Doctor of Philosophy

by

David L. Proctor

May 2009

TOPICS AND INSTRUMENTATION IN CHEMICAL REACTION DYNAMICS

David L. Proctor, Ph. D.

Cornell University 2009

The relative reactivity of methane excited in the antisymmetric stretching mode (ν_3) vs. the ground state in a prototype metal-insertion reaction, $Y + CH_4 \rightarrow YCH_2 + H_2$, has been measured in crossed molecular beam scattering. Under isoenergetic conditions where the sum of available vibrational and translational energy is held constant, the vibrationally excited state is at least 2.2 times more reactive than the ground state. The mid-infrared light source used to excite the methane is an Nd:YAG-pumped pulsed optical parametric oscillator/amplifier seeded with a continuous wave laser diode in the near infrared. The OPO/OPA system has an overall quantum efficiency of greater than 0.25 when using 350 mJ/pulse of pump light. The light source also includes a self-drilled vacuum spatial filter for the pump beam, enabling it to be used with pump lasers exhibiting structured beam profiles. Also presented are new piezo-electric bimorph actuators for use in high-speed pulsed valves used to generate pulsed molecular beams. They are more resistant to chemical attack than their commercial counterparts and deliver shorter pulses. The short pulse duration can provide greater beam intensities for a given pumping speed or reduce the pumping speed required to generate a given beam intensity.

BIOGRAPHICAL SKETCH

David Proctor was born on June 28, 1981 to Brooks and Susan Proctor of Littleton, Colorado, a suburb of Denver, and there began a lifetime interest in precision hardware as a bicycle mechanic. He graduated with honors from the Robert D. Clark Honors College at the University of Oregon where he performed research in the physical chemistry laboratory of Professor Andy Marcus, working on experiments in ultrafast spectroscopy. From there David arrived at Cornell with his wife, Katherine, and joined the laboratory of Professor H. Floyd Davis. There he developed light sources and pulsed valves for use in chemical dynamics experiments, and investigated the vibrational mode-specificity of the reaction of yttrium atoms with methane.

To Katie

It already is.

ACKNOWLEDGMENTS

First I need to thank Professor H. Floyd Davis, in whose laboratory I was able to bring a menagerie of tools and techniques to bear on problems in chemical reaction dynamics. He has demonstrated remarkable trust through his willingness to let me explore uncharted instrumental territory in search of that last factor of two in signal.

I also want to thank the members of the Davis group who took time out of their own random walks to show me how not to stub my toes during mine: Yumiko Nakatsuka, Mark Witinksi, and Mariví Ortiz-Suárez. Thanks are also due to the other graduate students with whom I've overlapped for their camaraderie in our efforts: Melania Oana, Steve Kroner, Dan Albert, and Martha Beckwith.

My thanks also go to the friends I've made in Ithaca: Jofish, Janet, Amy, Max, Meagan, Daegan, Nicole, and many others who have made my time at Cornell not just time at Cornell. I'd also like to thank Bob Snedeker and Nate Ellis, managers of the student machine shop, for their tutelage. It turns out yttrium machines much like copper but on the belt sander it sparks like titanium.

I thank my family, Brooks, Susan, Julie, Trent, Forrest, Judy, Nelson, Bridget, David, Olga, and many more for their support and perseverance with this endeavor which took me and Katie to the other side of the continent for five years. And finally I thank my wife Katie for sharing her life with me and making our time here about more than academics. We started graduate school and our marriage at the same time and I can't say from which I've learned more.

TABLE OF CONTENTS

BIOGRAPHICAL SKETCH iii
DEDICATION iv
ACKNOWLEDGEMENTS v
TABLE OF CONTENTS vi
LIST OF FIGURES vii
1. A HIGH-EFFICIENCY OPTICAL PARAMETRIC OSCILLATOR/AMPLIFIER OPERATING IN THE MID-INFRARED 1
1.1 Introduction 1
1.2 Self-drilled Vacuum Spatial Filter 1
1.3 Injection-seeded Optical Parametric Oscillator 5
1.4 Optical Parametric Amplifier 9
1.5 Application: Mid-infrared Cavity Ringdown Spectroscopy in a Supersonic Jet 11
1.5 Application: Vibrational Pumping of Methane in Crossed Molecular Beams Scattering 13
1.6 Acknowledgements 14
1.7 References 16

2. VIBRATIONAL VS. TRANSLATIONAL ENERGY IN PROMOTING A PROTOTYPE METAL-HYDROCARBON REACTION[*] 17
2.1 Introduction 17
2.2 Results 20
2.3 Discussion 26
2.4 Experimental Methods 29
2.5 Acknowledgements 32
2.6 References 33

3. IMPROVED PIEZOELECTRIC ACTUATORS FOR USE IN HIGH-SPEED PULSED VALVES 36
3.1 Introduction 36
3.2 Actuator Designs and Construction 37
3.3 Results 41
3.4 Discussion 45
3.5 Acknowledgements 46
3.6 References 47

[*] Original publication: Proctor, D. L.; Davis, H. F. *Proceedings of the National Academy of Sciences* **2008** *105*, 12673.

LIST OF FIGURES

Figure #	**Page #**	**Figure Title**
1.1	4	Beam Profiles Before & After Spatial Filtering
1.2	6	Schematic Layout of the OPO/OPA
1.3	8	OPO Conversion Efficiency
1.4	10	OPA Conversion Efficiency
1.5	12	Cavity Ringdown Absorption Spectrum of Jet-Cooled Methane
1.6	14	Methane Saturation Curve in Crossed-Beams Scattering
2.1	19	Energy Level Diagram of $Y + CH_4 \rightarrow YCH_2 + H_2$
2.2	21	OPO-off and OPO-on Collision Energy Distributions
2.3	22	YCH_2 Lab Angular Distribution and Kinetic Energy Release
2.4	24	YCH_2 Time-of-Flight Distributions
2.5	25	YCH_2 Signal as a Function of OPO Energy
3.1	38	Piezoelectric Actuator Designs
3.2	43	Beam Intensity Profiles

CHAPTER 1

A HIGH-EFFICIENCY OPTICAL PARAMETRIC OSCILLATOR/AMPLIFIER OPERATING IN THE MID-INFRARED

Introduction

Pulsed, injection-seeded optical parametric oscillators (OPOs) and amplifiers (OPAs) can provide narrow bandwidth light suitable for spectroscopy at wavelengths from the ultraviolet through the infrared. In the infrared there are few tunable high power light sources available, and OPO/OPA systems represent the best option when high intensity, narrow bandwidth IR light is required. Here we present an OPO/OPA system optimized for high spectral brightness in the mid-infrared, and a vacuum spatial filter that allows the OPO to be pumped by a Q-switched Nd:YAG laser with a suboptimal beam profile.

Self-drilled Vacuum Spatial Filter

Efficient operation of a pulsed optical parametric device (generator, oscillator, amplifier, etc.) requires a smooth spatial beam profile of near uniform intensity from the pump laser. This is because for many optical crystals and coatings, the irradiance threshold for optical damage from the pump laser is not much higher than the threshold for the desired parametric process, so collimated pump beams are employed and larger spot sizes must be used with higher pump powers. In the worst case scenario hot spots in the pump beam may exceed the damage threshold before the rest of the pump beam has achieved the parametric threshold. In less extreme cases a poor pump profile will result in a lower than expected conversion efficiency and a poor parametric beam profile, making subsequent amplification or conversion steps difficult or impossible. Current flashlamp-pumped Nd:YAG laser designs can have excellent beam profiles, but many older lasers that are still in service, especially those

that were factory-optimized for beam power rather than beam quality, exhibit beam profiles unsuitable for pumping a parametric device. They often exhibit a pattern of concentric rings from diffraction on one or more apertures in the laser. These defects also appear in many lasers which operate at repetition rates greater than 10 Hz, regardless of vintage. The greater thermal effects in these lasers are often less precisely compensated for than in their 10 Hz brethren. Non-uniformities in the beam profile can, however, be significantly reduced with a spatial filter.

A spatial filter leverages Fourier optics to remove high spatial frequency components of a laser beam profile. For a collimated laser beam, the image at the focal plane of a lens is the two-dimensional Fourier transform of the beam profile one focal length behind the lens. This image appears as a focal spot because a beam always consists primarily of low spatial frequencies, which are concentrated at the frequency domain origin (the beam axis) in the focal plane. Higher spatial frequency components in the beam profile result in a broadening of this spot. A spatial filter is an aperture that blocks the transmission of these higher frequencies while allowing the low frequencies to pass. [1]

Simple spatial filters consisting of a lens and a pinhole are commonly used with low power lasers to create a nearly perfect spherical wavefront, required, for example, for recording holograms, but constructing a filter for use with a high energy pulsed laser requires special considerations. First, the field strength at the focus from such a laser is great enough to ionize air. Light is scattered by the resulting plasma, producing a poor and unstable beam profile downstream. We solve this problem by placing the focus in a vacuum. The pinhole is also of concern because these lasers are capable of ablating most materials, resulting in short aperture lifetimes. To address this we developed a simple, self-aligning vacuum spatial filter in which the laser drills its own aperture in a material resistant enough to ablation that only the most intense

part of the focal spot drills through. This approach has been used in at least one previous instance,[2] in that case to remove amplified stimulated emission from a picosecond pulse train before amplification.

Our vacuum spatial filter was constructed to modify the beam profile of an older injection-seeded 30 Hz laser (Continuum Powerlite 9030) which displays the diffraction rings mentioned above. The filter is a unity magnification design using two 250 mm focal length plano-convex lenses anti-reflection coated at 1064 nm (10-5 scratch-dig, CVI Laser), spaced approximately 500 mm apart. These two lenses also serve as the input and output windows to a vacuum chamber held at less than 10^{-6} torr by a 60 l/s turbomolecular pump. Mounted at the focal spot is the aperture substrate, a disc of Macor machinable glass ceramic approximately 0.5 mm thick. The precise thickness was not found to be important. The vacuum flange holding the output lens is attached to the chamber with a bellows-sealed linear translator, allowing the distance between the focus and lens, and hence the collimation of the output beam, to be adjusted. The filter is aligned by first pumping the chamber down without an aperture substrate installed to position the filter chamber relative to the pump laser. The filter chamber is placed such that the pump laser beam traverses the chamber without clipping and that back-reflections from the lenses are sufficiently off-axis to avoid feedback into the laser. The chamber is then vented, an aperture substrate is installed, and the chamber pumped down again. The aperture is drilled by turning on the pump laser and allowing the beam to drill its own aperture by ablating material at the focus. At full power, 450 mJ per pulse for this laser, the procedure takes approximately 100 shots. Figure 1.1 shows beam profiles recorded before and after the installation and drilling of an aperture, as well as histograms of the per-pixel intensities in the profile images.

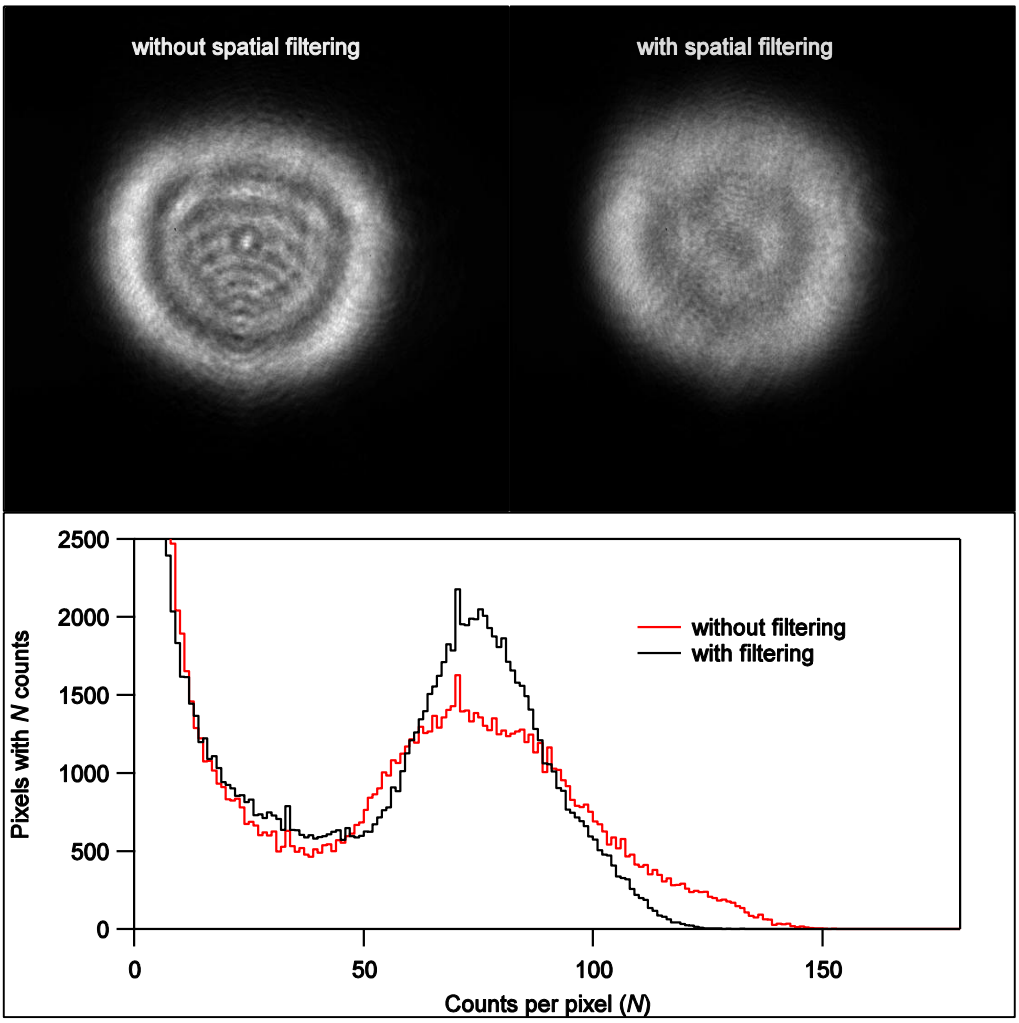

Figure 1.1: Beam profiles of the Continuum Powerlite 9030 before and after spatial filtering, with histograms of the pixel height distributions showing a higher, narrower peak around the average pixel height for the filtered beam.

Both images display small amplitude diffraction patterns from dust on the 2:1 reducing telescope and attenuation optics mounted to the profiling camera (Spiricon Scorpion). The effects of filtering are obvious: the fringe pattern is significantly reduced both in amplitude and frequency. The ratio of the highest intensity inside the beam to the lowest is reduced by 30% with the filter installed. The total power of the filtered beam is 98% of that of the unfiltered beam, not counting the extra loss of less than 1% from traversing the four anti-reflection coated lens surfaces. A perfect "top hat" profile, with a uniform intensity within the beam and no intensity outside it, would show only two occupied bins on a histogram such as the ones in Figure 1.1, one at the average beam intensity and one at zero. The filtered beam is closer to this ideal, showing a narrower peak around the average intensity of 75 counts per pixel and a highest intensity of approximately 125 counts per pixel vs. 150 for the unfiltered beam. The attenuation of the hottest parts of the beam and filling in of the coolest parts while maintaining nearly all of the beam power demonstrates that the self-drilled aperture is nearly ideal for this application: a poor beam profile has been transformed into a usable one without sacrificing photons better spent on parametric processes. A single aperture lasts over a month of daily operation before the beam quality decays. This is probably due to the long-term pointing drift of the laser causing shifts in the position of the focus and eventually enlarging the aperture.

Injection-seeded Optical Parametric Oscillator

The finite acceptance angle for critical phase-matching optical parametric process in non-linear crystals normally results in bandwidths for the generated signal and idler beams between 1 cm^{-1} and 100 cm^{-1}. To reduce this bandwidth, a small amount of narrow-bandwidth light can be injected into the oscillator to give one wavelength within the unseeded bandwidth a head start in the race for gain inside the cavity. Our optical parametric oscillator/amplifier is conceptually similar to an

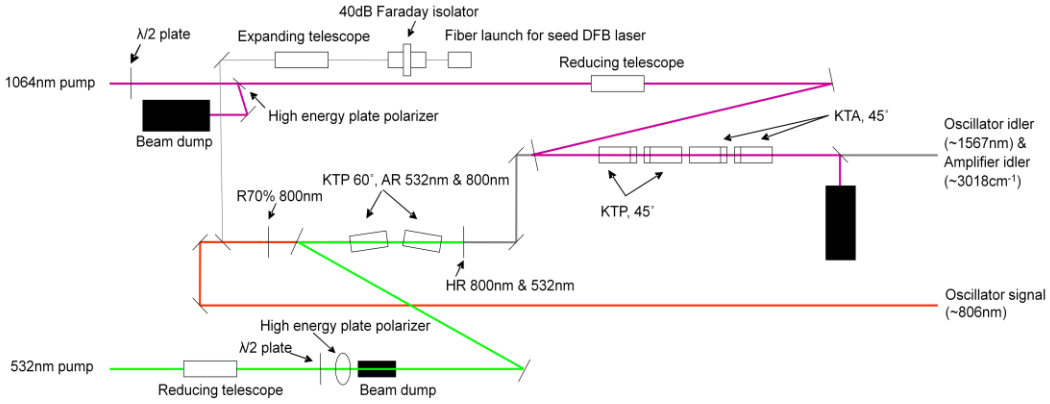

Figure 1.2: Schematic layout of the injection-seeded OPO/OPA system.

existing design[3] in that it is comprised of a seed source, an OPO pumped at 532 nm, and an OPA pumped at 1064 nm. The pump beam is partially frequency doubled in a type 1 crystal after being filtered, and the 532 nm and 1064 nm beams separated with a dichroic beamsplitter before being sent to the OPO/OPA system.

Differences from that system are the use of a distributed feedback diode (DFB) laser as the seed source, the use of a resonant cavity for the OPO, and the addition of two more crystals in the OPA. The system is shown schematically in Figure 1.2. The seed laser is a commercial fiber-coupled DFB laser (NEL) operating at 1568 nm with 10 mW output power and 10 MHz bandwidth. It is mounted in a housing which acts as a heat sink and provides protection from external fields (ILX Lightwave LDM-4980). The wavelength of the DFB laser is measured with a fiber-coupled wavemeter (Advantest TQ8325) to which 1% of the light is sent via a fiber splitter (Newport). The wavelength is determined by the diode injection current, stabilized to 0.05 mA with a precision current supply (ILX Lightwave LDX-3220), and by the diode temperature, stabilized to 0.001 ºC by a precision PID temperature controller (ILX Lightwave LDT-5948) interfaced to the thermoelectric cooler and thermistor built into the DFB laser package. The fine tuning of the laser wavelength is accomplished by adjusting the temperature set point of the controller PID circuit. The tuning curve is

extremely linear with a slope of 0.1135 ± 0.0002 nm/ºC and has been operated at temperatures from 10 ºC to 45 ºC. The light from this laser travels to the optical bench via a single mode fiber, is collimated with a fiber launch, directed through a free-space Faraday isolator (OFR), then expanded with a telescope to approximately 7 mm diameter and sent into the OPO. A segment of the optical fiber is wrapped twice around a 50 mm diameter circular form which serves as a simple polarization controller via stress-induced birefringence. The power transmitted by the isolator is maximized by rotating the form. Although imprecise, this arrangement routinely results in more than 90% of the seed laser power traversing the isolator. A single isolator, with approximately 40 dB rejection, is insufficient to protect a laser diode from the feedback presented by the pulsed OPO. The DFB laser package also includes a built-in isolator and together these isolators can protect the diode from feedback at MW-scale peak powers.

The OPO stage generates light at the signal wavelength, 806 nm, which is the difference frequency between the 532 nm pump and 1569 nm seed beams, while also pulse-amplifying the seed/idler wavelength. The conversion process occurs in a pair of 7 mm × 7 mm × 15 mm KTP crystals cut at 60º in the X-Z plane for type 2 phase matching and anti-reflection coated at 532 nm and 800 nm. They are mounted on computer-controlled rotation stages moving in the horizontal plane in a counter-rotating, walkoff-compensating geometry[4]. The polarizations of the OPO beams are vertical for the pump and seed/idler beams, and horizontal for the signal beam. The oscillator consists of a pair of mirrors, one coated for high reflectivity at both 532 nm and 800 nm, and one with 80% reflectivity at 800 nm. The pump beam is folded into the cavity on a mirror tilted off-axis and coated to reflect at 532 nm on the front surface with no coating on the back. The pump intensity is controlled with a half-wave plate and polarizer combination upstream of a telescope which reduces the beam

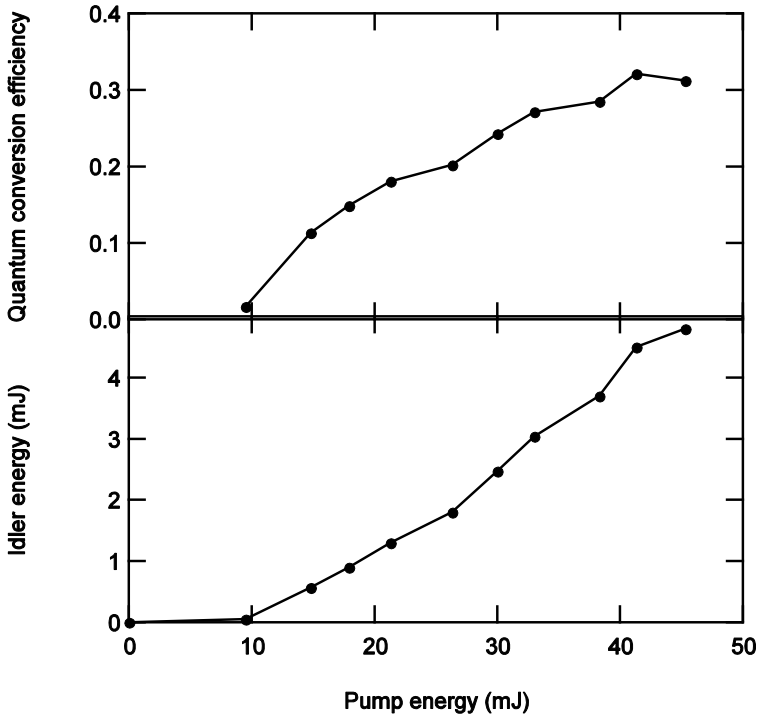

Figure 1.3: OPO idler output energy and conversion efficiency.

diameter to 4 mm. In this cavity configuration the seed light at the idler wavelength passes straight through the cavity, suffering losses only from Fresnel reflections. Oscillation occurs on the signal wavelength exclusively, similar to the "medium finesse" oscillator described by Kulatilaka et. al[5]. Because the pump beam is retroreflected and thus double-passed through the crystals, the resonated signal beam is amplified in both directions. The 80% 800 nm reflector ensures that a majority of the signal light leaves the cavity by one end, but the idler energy leaves by both. It is because of this that the Faraday isolator in the seed beam path is required to protect the DFB laser: an amplified idler beam is sent directly back towards the fiber launch. Despite these complications arising from double-passing the pump, the lower oscillation threshold, higher conversion efficiency, and lower output beam divergence that double-passing provides results in higher energies from the downstream OPA

stage. The total cavity length is 300 mm. Slightly higher gain and a lower oscillation threshold were observed with a shorter cavity, but it made the threshold for free-running operation so low that the OPO would not seed at pump energies high enough to get good conversion efficiency. The threshold behavior of the OPO is shown in Figure 1.3. The pump energy threshold for oscillation is 9 mJ/pulse. The pump conversion quantum efficiency appears to plateau at about 32% with 40 mJ/pulse pump energy. Seeded operation is confirmed by passing the signal beam through a 50 GHz free-spectral range solid etalon and, using an IR viewer, observing sharp rings which disappear when the seed beam is blocked. Good seeding performance was observed with seed powers as small as 2 mW. The idler beam which exits the OPO through the pump retroreflecting mirror is aligned in to the OPA with a pair of steering mirrors. The conversion efficiencies shown in Figure 1.3 should be regarded as lower limits because the pump energy was measured just in front of the OPO crystals, but the idler energy was measured "as delivered" to the OPA crystals, after having passed though the cavity mirror, two steering mirrors, and the OPA pump fold mirror. It also does not include the idler energy that is directed back towards the seed laser fiber launch.

Optical Parametric Amplifier

The OPA stage amplifies the seed/OPO idler frequency while also generating the 3.3 μm difference frequency between the 1064 nm pump and 1568 nm seed/OPO idler beams. It is a single-pass amplifier using four 7 mm × 7 mm × 15 mm non-linear crystals. Two of these are KTP and the other two are KTA, all cut at 45º in the X-Z plane and anti-reflection coated for 1064 nm. The pump energy is again controlled by a half-wave plate and polarizer combination before a telescope reduces the beam diameter to 4 mm. The depleted pump beam is separated from the signal and idler with a long-pass filter on a CaF_2 substrate (LaserVision). Here the polarizations are

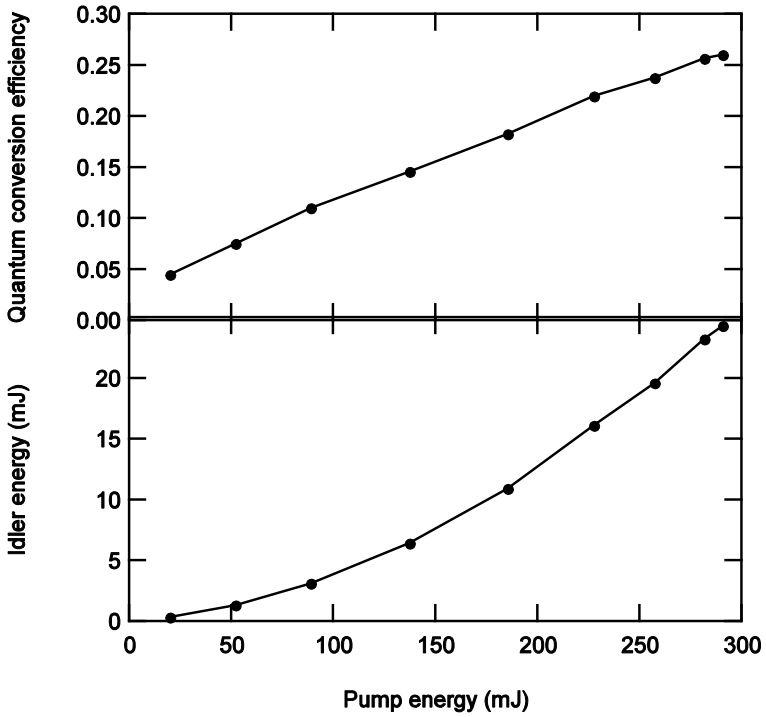

Figure 1.4: OPA idler output energy and conversion efficiency.

horizontal for the 1064 nm pump and 3.3 μm idler and vertical for the 1568 nm seed/signal. All four crystals are mounted on vertical rotation stages. The KTP mounts are under computer control while the KTA stages were added later and are manually actuated. This arrangement reflects a compromise between automated scanning control and ease-of use. The computer controlled stages are convenient for scanning over relatively large wavelength ranges, and with the KTP crystals alone the amplifier produces 1.8 mJ/pulse at 3.3 μm. This is more than enough for spectroscopic investigations. When an absorption feature has been identified and tuned to, the manual stages allow for quick maximization of the output power up to 24 mJ/pulse. The acceptance bandwidth for critical phase matching in both the OPO and the OPA still allows the seed laser to be scanned over approximately 0.25 nm without tuning any of the crystal angles. The amplifier's 3.3 μm production as a function of pump energy is shown in Figure 1.4. The quantum efficiency shown there should also

be viewed as a lower limit because the OPA pump energy was measured directly before the crystals but the idler energy was measured after having passed through the pump separation mirror, a CaF_2 prism to separate the signal from the idler beams, and a gold-coated steering mirror. Even with pump energies of 300 mJ per pulse the amplifier conversion efficiency hasn't leveled off. If larger pump energies are available, even greater conversion efficiencies can be expected.

Application: Mid-infrared Cavity Ringdown Spectroscopy in a Supersonic Jet

To test the OPO/OPA system we used the 3.3 μm output of the OPA to perform mid-IR pulsed cavity ringdown absorption spectroscopy on a supersonic jet. The spectrometer consists of a vacuum chamber evacuated by a 5000 l/s vapor diffusion pump and containing a fast piezoelectrically actuated pulsed valve[6] synchronized with the pump laser Q-switch. Extensions on the chamber hold a pair of 1-m radius of curvature concave mirrors 99.97% reflective at 3.3 μm (Los Gatos Research) in tilt-adjustable mounts, forming a stable cavity approximately 1.3 m long. The nozzle of the pulsed valve is held 5 cm away from the cavity axis. The 3.3 μm beam from the OPA, attenuated to 1 mJ/pulse, was injected in one end of the cavity using a 1-m focal length mode-matching lens. The light escaping the other end of the cavity was measured with a liquid nitrogen cooled InSb photodiode (InfraRed Associates) through two bandpass filters (JDSU) which remove pump and signal light from the OPA that is scattered from the surface of the CaF_2 prism onto the detection axis. Normally this small amount of light wouldn't pose a problem, but in the cavity ringdown experiment the 3.3 μm light being detected is only what has been transmitted by two high-reflectivity mirrors that are transparent to the other wavelengths present in the OPA. In this case only one 3.3 μm photon in 10^7 makes it to the detector. The impulse response function of this detector is approximately 3 μs full-width at half-maximum, approximately one-fifth the maximum ringdown time

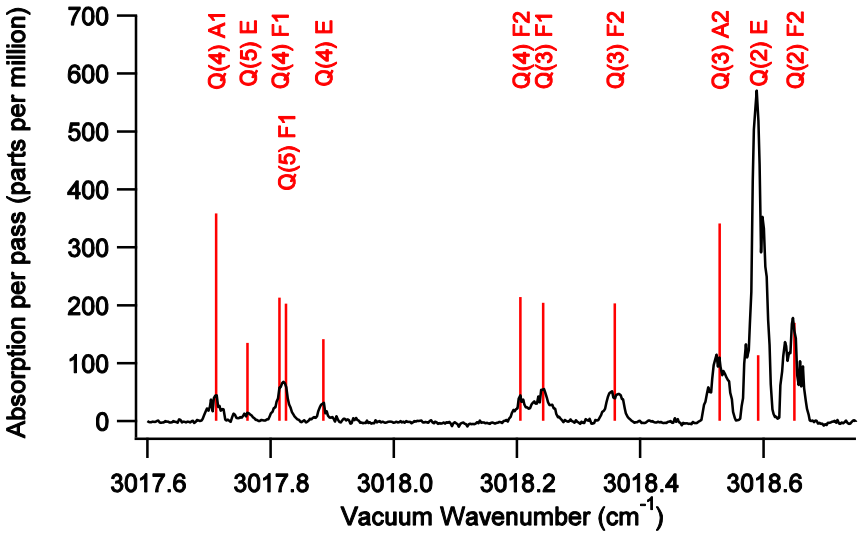

Figure 1.5: Cavity ringdown absorption spectrum of a portion of the methane ν_3 symmetric stretch Q-branch in a supersonic jet. The stick spectrum is of predicted positions and intensities at 298 K, labeled by line designation and nuclear modification.

constant with the chamber evacuated. The relatively short ringdown signals are therefore distorted by this impulse response. To compensate for this, the signals are digitized and fit to an idealized ringdown convolved with the detector impulse response function using the Levenberg-Marquardt non-linear least squares algorithm. The time constant of this idealized trace was recorded as the ringdown time constant. Figure 1.5 shows a portion of the methane ν_3 Q-branch recorded with this instrument, along with the positions, relative intensities at 298 K, and nuclear spin modification of the lower states for expected transitions.[7] The spectrum shows large intensity deviations from 298 K equilibrium due to rotational cooling in the jet. In particular the very large relative intensity of the Q(2) transition in the *E* modification is evidence of the lack of nuclear relaxation during the expansion. The ground vibrational state population in the *E* modification at 298 K equilibrium is concentrated upon jet cooling in $J = 2$, the lowest rotational state in the modification, rather than relaxing to $J = 1$ or

$J = 0$. The full-width at half-maximum bandwidth of the OPA output, taken as the width of the lone transitions, is approximately 950 MHz.

This bandwidth was confirmed by laser-induced fluorescence measurements on a collimated beam of vanadium atoms using the frequency-doubled signal output of the OPO. In these measurements the width of hyperfine transitions was measured to be 1.35 GHz, which corresponds to 950 MHz broadened by a factor of 1.41 from the frequency-doubling process. This bandwidth is larger by a factor of approximately three than the transform limit if the output pulse has the same duration as that of the OPO pump.

Application: Vibrational Pumping of Methane in Crossed Molecular Beams Scattering

We recently used the OPO/OPA to pump the methane ν_3 antisymmetric stretch vibrational mode in a recent investigation of methane's mode-specific reactivity with yttrium atoms.[8] A collimated methane molecular beam was crossed with a collimated beam of yttrium atoms at a collision energy below the threshold for reaction. The 3.3 μm beam from the OPA, tuned to the ν_3 Q(1) line, was crossed at right angles with the methane beam just upstream of the collision region. The YCH_2 reaction product signal as a function of the incident 3.3 μm energy is shown in Figure 1.6. The fast initial rise is due to the most intense parts of the OPA beam profile saturating the transition at low total energy, and the slower increase in signal at higher energies comes from increasing saturation even in the less intense parts of the profile. The very high conversion efficiency of the OPO/OPA system produces energies well in excess of that required to observe saturation in an allowed transition, but the reality of imperfect beam profiles means much greater energies are required to achieve saturation within the entire beam spot. At the energies our OPA provides, pulse-to-pulse energy fluctuations contribute almost no extra noise to the experiment. The

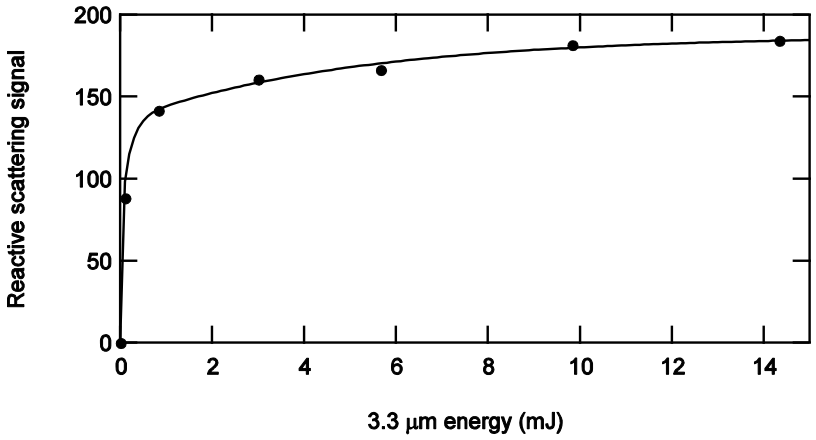

Figure 1.6: Reactive scattering signal in a crossed molecular beam experiment where no reaction occurs without the energy provided by absorption of a photon produced by the OPA.

OPA also, by necessity, produces very high pulse energies at its signal wavelength near 1.5 μm. With the system seeded at an appropriate wavelength this light can be used to excite overtone and combination bands in many hydrocarbons. The intensities provided by this OPA are adequate to nearly saturate those transitions despite their absorption cross-sections being smaller than those of the fundamental transitions by a factor of approximately 250.

In summary, we have constructed an OPO/OPA system with more than 25% conversion efficiency in converting the 1064 nm output of an injection-seeded Q-switched Nd:YAG laser to tunable, narrow-band light in the near- and mid-infrared. The system is seeded with a commercial DFB laser, providing wavelength stability sufficient for long-duration experiments. It routinely remains tuned to a single rovibrational transition for the 12-hour duration of a reactive scattering experiment

Acknowledgements

We wish to thank Dr. Dean R. Guyer (dba LaserVision) for helpful advice concerning optical materials and Dr. Waruna Kulatilaka for helpful discussions regarding laser diode instrumentation. This work was supported by the National

Science Foundation Grant CHE-0316296 and the United States Department of Energy Grant DE-FG02-00ER1505095.

REFERENCES

[1] Guenther, R. D. *Modern Optics*; John Wiley & Sons: New York, 1990.

[2] Bodey, A. J.; Hirst, G. J.; Shaikh, W. In *Central Laser Facility Annual Report 2001/2002*; Science and Technology Facilities Council: Rutherford Appleton Laboratory, UK, 2002; p 200; http://www.clf.rl.ac.uk.

[3] Bosenberg, W. R.; Guyer, D. R. *Journal of the Optical Society of America* **1993,** *10*, 1716.

[4] Armstrong, D. J.; Alford, W. J.; Raymond, T. D.; Smith, A. V.; Bowers, M. S. *Journal of the Optical Society of America B* **1997**, *14*, 460.

[5] Kulatilaka, W. D.; Anderson, T. N.; Bougher, T. L.; Lucht, R. P. *Applied Physics B* **2005**, *80*, 669.

[6] Proch, D.; Trickl, T. *Review of Scientific Instruments* **1989** *60*, 713.

[7] Rothman; Jacquemart, D.; Barbe, A.; Chris Benner, D.; Birk, M.; Brown, L. R.; Carleer, M. R; Chackerian Jr., C.; Chance, K.; Coudert, L. H.; Dana, V.; Devi, V. M.; Flaud, J.-M.; Gamache, R. R.; Goldman, A.; Hartmann, J.-M; Jucks; Maki, A. G.; Mandin, J.-Y.; Massie, S. T.; Orphal, J.; Perrin, A.; Rinsland, C. P.; Smith, M. A. H.; Tennyson, J.; Tolchenov, R. N.; Toth, R. A.; Vander Auwera, J.; Varanasi, P.; Wagner, G. *Journal of Quantitative Spectroscopy and Radiative Transfer* **2005** *96*, 139.

[8] Proctor, D. L.; Davis, H. F. *Proceedings of the National Academy of Sciences* **2008** *105*, 12673.

CHAPTER 2

VIBRATIONAL VS. TRANSLATIONAL ENERGY IN PROMOTING A PROTOTYPE METAL-HYDROCARBON REACTION

Introduction

The concepts of early and late potential energy barriers made it possible to rationalize in simple, intuitive terms the roles of reactant translational and vibrational energy in promoting atom + diatom reactions.[1] The observation of mode- and bond-specific effects in gas phase reactions such as $Cl + CH_4 \rightarrow HCl + CH_3$ and $Cl + H_2O \rightarrow HCl + OH$ have illustrated that the dynamics of polyatomic systems involving multiple vibrational degrees of freedom can also be highly sensitive to the reactant vibrational state.[2,3]

In a recent study, Yan and coworkers provided the first direct comparison of C-H reactant vibrational energy to reactant translational energy in promoting the $Cl + CHD_3 \rightarrow HCl + CD_3$ abstraction reaction.[4] Although C-H antisymmetric vibrational excitation enhanced reactivity, it was found to be somewhat *less* effective than an equivalent amount of reactant translational energy. However, CHD_3 bending excitation induced by thermal excitation was somewhat *more* effective in promoting reaction than an equivalent amount of translational energy. For gaseous polyatomic systems, different forms of reactant energy may not be equivalent in facilitating passage through the transition state for atom transfer.[2-5]

The dissociative adsorption of methane (CH_4) on a metal surface is the rate-limiting step in the steam re-forming of methane, used to produce ≈9 million tons of hydrogen annually in the United States. It is well-established that reactant translational *and* vibrational excitation are both effective in promoting this activated

process.[6] Significant mode- and bond-specific effects have been observed for this class of reaction. Smith and coworkers showed that antisymmetric CH_4 vibrational excitation (ν_3) is somewhat more effective than an equivalent amount of translational energy in promoting reaction on a Ni(111) surface,[7] in contrast to earlier work on Ni(100)[6] and Pt(111),[8] where translational energy was more effective in promoting reaction. Juurlink *et. al.* demonstrated that CH_4 overtone bending excitation ($3v_4$) is much less effective than v_3 on Ni(100) and Ni(111), despite the higher energy of $3v_4$.[9] Maroni and coworkers found that CH_4 symmetric excitation (v_1) is about an order of magnitude more effective than antisymmetric stretching (v_3) in promoting reaction on Ni(100) at nearly identical total energies.[10] The latter result is particularly striking because it demonstrates that, even for a complex polyatomic reaction at the gas-solid interface, two reactant vibrational states that differ only in the relative phases of atomic motions can have profoundly different reactivities.

The activation of hydrocarbon C-H and C-C bonds by transition metal complexes is a topic of considerable current interest.[11,12] Insight into the factors controlling the kinetics and thermodynamics of these processes has been derived through electronic structure theory.[13] Unfortunately, the presence of multiple ligands in transition metal complexes makes theoretical calculations difficult. Consequently, substantial effort has been devoted to carrying out calculations on model systems involving insertion of isolated transition metal *atoms* into C-H and C-C bonds.[14,15] Interestingly, recent theoretical work on the dynamics of the dissociative adsorption of methane on Ir(111)[16] and Ni(111)[17] surfaces indicate that the metal lattice undergoes reconstruction during reaction, with a local surface metal atom undergoing significant (0.6 Å) displacement outward from the surface. Understanding the reactivity of isolated transition metal atoms with methane may thus provide insight into the dissociative adsorption process.

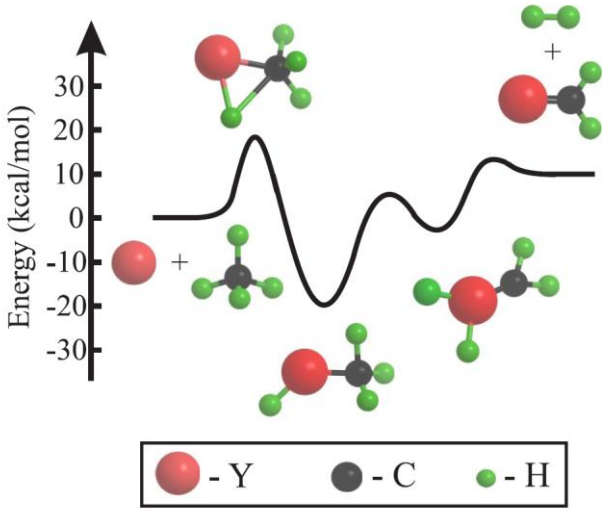

Figure 2.1: Schematic energy level diagram for Y + $CH_4 \rightarrow YCH_2 + H_2$ reaction.

Early second-row transition metal atoms have few valence electrons, (e.g. $5s^2 4d^1$ for Y), yet form strong M-H and M-C bonds.[14,15] However, neutral metal atoms encounter substantial potential energy barriers for insertion into C-H bonds of saturated hydrocarbon molecules.[14,15] One of the simplest prototypical neutral bimolecular reactions involving a transition metal center with methane is Y + $CH_4 \rightarrow HYCH_3 \rightarrow YCH_2 + H_2$ (Figure 2.1). This reaction involves initial insertion of the metal center into a C-H bond of methane by passage over a potential energy barrier calculated by Wittborn and coworkers to lie 20.5 kcal/mol above the reactants.[14] For the analogous reaction involving ethane (C_2H_6), the potential energy barrier for C-H insertion was measured to be 19.9 ± 3.0 kcal/mol.[18] As expected, collisions at translational energies below the barrier were unreactive, but formation of both $YC_2H_4 + H_2$ and $YH_2 + C_2H_4$ was observed at collision energies above the barrier.[18] For Y + CH_4, the initial insertion step can be viewed as involving elongation of a C-H bond in the CH_4 reactant (Figure 2.1) with simultaneous formation of two new bonds producing $HYCH_3$. By analogy with the surface experiments, and because C-H stretching is likely to be an important component of the reaction coordinate, C-H

vibrational excitation might be effective in promoting insertion. However, the antisymmetric CH_4 stretching mode (ν_3) is a normal mode involving motion of all four atoms in methane, whereas insertion involves a local interaction with a single C-H bond. To date there has been no systematic study in which translational energy is compared to vibrational energy in promoting an insertion reaction.

Results

We conducted crossed molecular beam reactive scattering experiments between Y atoms and ground state CH_4 at beam velocities providing 23.8 ± 1.5 kcal/mol translational energy and between Y and CH_4 ($\nu_3 = 1$) at beam velocities providing 15.1 ± 0.9 kcal/mol of translational energy. Figure 2.2 shows the total reactant energy distributions for the two sets of experiments. The vibrational energy in the second experiment, provided by absorption of a 3,018 cm^{-1} photon produced by an infrared optical parametric oscillator (OPO), makes the total energy essentially identical in each experiment. Mass-selected time-of-flight (TOF) distributions of YCH_2 reaction products were recorded at several laboratory angles relative to the beams for both experiments. Calculated TOF distributions based on iteratively adjusted center-of-mass (CM) frame product translational energy and angular distributions were fit to the data by using forward convolution over known beam velocity distributions and instrument functions.

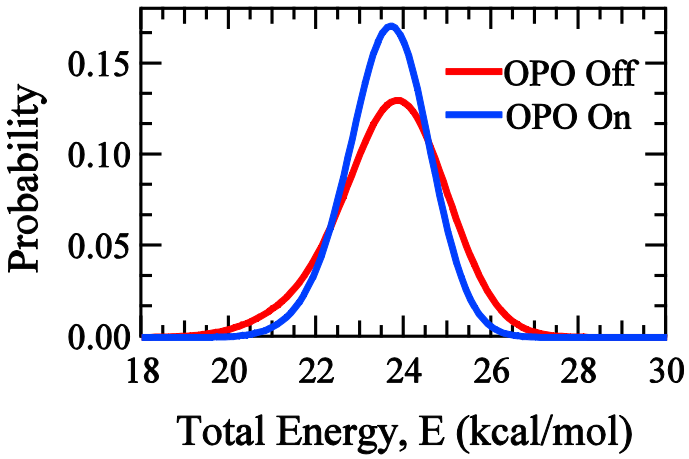

Figure 2.2: Probability distribution function for total reactant energy in "OPO Off" and "OPO On" experiments. In OPO Off experiments, all reactant energy is translational; in OPO On experiments, total reactant energy includes 8.63 kcal/mol of vibrational excitation in the CH4 antisymmetric stretch (v_3) vibrational mode.

Figure 2.3 shows the laboratory angular distribution of YCH_2 products at the 23.8 kcal/mol collision energy, as well as the CM translational energy distribution used in the fit. The CM angular distribution, $T(\theta)$, was isotropic as anticipated for a reaction involving complexes with lifetimes longer than their rotational periods. Figure 2.4 shows the TOF distributions for the YCH_2 products. At this collision energy (i.e., above the barrier), reaction of ground-state CH_4 leads to formation of $YCH_2 + H_2$, with the product translational energy $P(E)$ peaking near 3 kcal/mol and extending to 11 kcal/mol, with $\langle P(E) \rangle$ = 3.6 kcal/mol. The TOFs and lab angular distribution for the 15.1 kcal/mol collision energy with vibrational excitation were fit using the same $P(E)$ and CM angular distribution and appear similar.

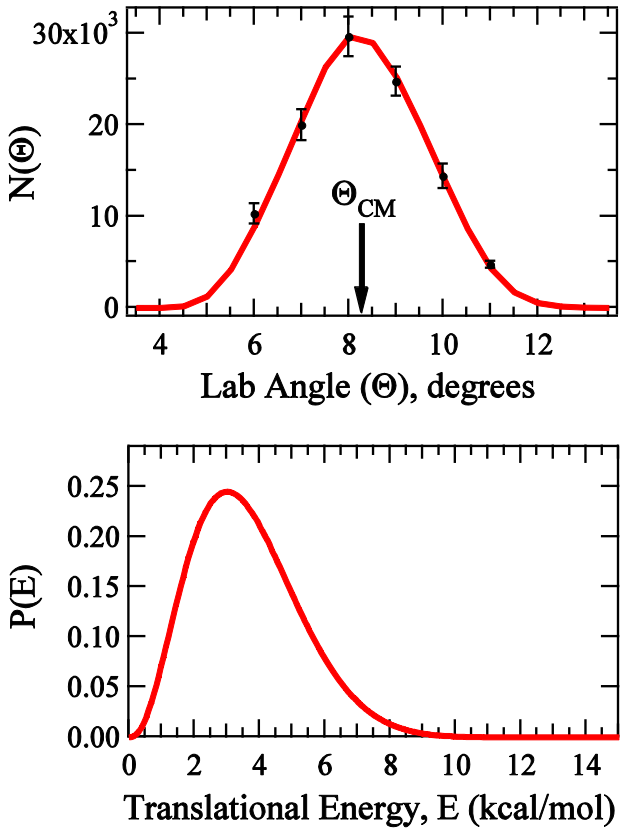

Figure 2.3: Laboratory angular distribution with marked center-of-mass scattering angle and product translational energy release distribution, *P(E)* for Y + CH_4 → YCH_2 + H_2 at E_{coll} = 23.8 kcal/mol with OPO Off. Data in black, fit in red, and error bars are 90% confidence intervals.

We have found that the reaction cross section rises sharply with reactant collision energy. The dependence of the reactive signal on collision energy places the potential energy barrier for reaction at 20 ± 3 kcal/mol. The uncertainty in this value results primarily from the spread in collision energies for each experiment and from the presence of spin orbit excited $Y(^2D_{1/2})$, which lies 1.5 kcal/mol above the ground $Y(^2D_{3/2})$ state, in the atomic beam. The product translational energy release data place the $YCH_2 + H_2$ product asymptote ≈11 kcal/mol above the reactants. This is consistent with product energetics calculated by using the results of recent theoretical work that places this value near 12 kcal/mol.[19] The rate-limiting step in the reaction thus corresponds to passage of the system over the initial barrier for C-H insertion.

At a nominal mean collision energy of 18.6 kcal/mol, weak product signal was observed for ground-state CH_4 molecules. At a collision energy of 15.1 kcal/mol, no reaction was observed without OPO irradiation. Inelastic scattering experiments indicated that, at this collision energy, the nonreactively scattered Y atoms are strongly forward-scattered in the CM frame, indicating the occurrence of direct inelastic scattering without appreciable formation of long-lived YCH_4 complexes. The absence of complex formation at collision energies below the barrier is anticipated because neutral metal-alkane σ-complexes are bound by no more than 1-2 kcal/mol.[20] At this collision energy, which is well below the C-H insertion barrier for ground vibrational state CH_4 molecules, a strong YCH_2 signal is observed when the CH_4 molecules are optically pumped to the C-H antisymmetric stretching level (ν_3) just prior to collision. The observed YCH_2 signal level as a function of OPO pulse energy (Figure 2.5) indicates that the transition is easily saturated because of the narrow bandwidth of the OPO. Thus C-H vibrational excitation opens up reactions of colliding pairs at collision energies that were completely unreactive for unexcited methane.

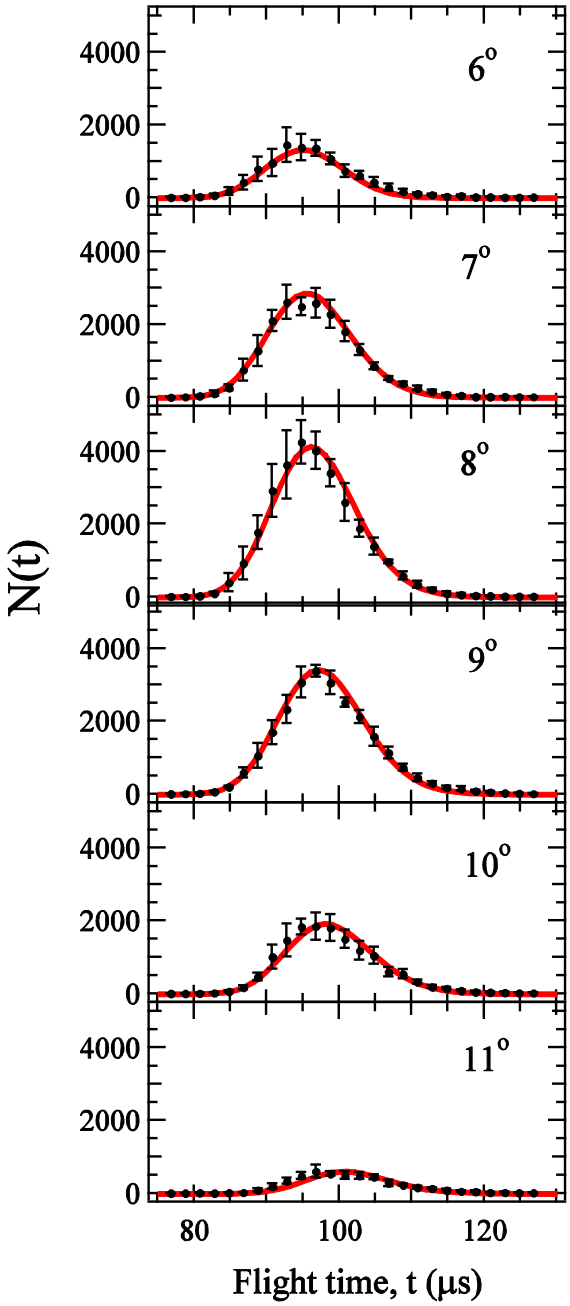

Figure 2.4: Laboratory time-of-flight distributions for YCH_2 products at indicated laboratory angles with OPO Off. Filled circles denote experimental data and solid line is calculated distribution using *P(E)* from Figure 2.2 and isotropic center-of-mass angular distribution *T(Θ)*. Data in black, fit in red, and error bars are 90% confidence intervals.

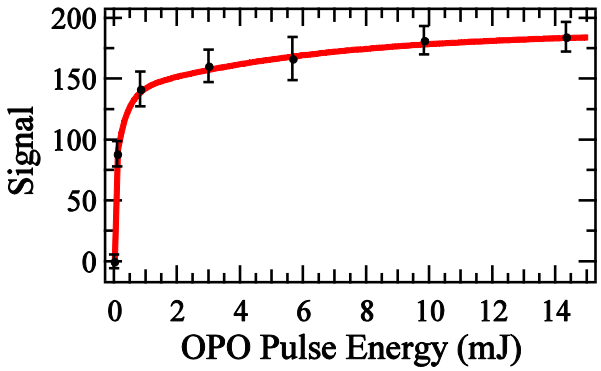

Figure 2.5: Saturation curve showing YCH_2 signal recorded at laboratory center-of-mass angle as a function of OPO pulse energy. Data in black, fit in red, and error bars are 90% confidence intervals.

In order to obtain quantitative insight into the relative efficacy of *vibrational vs. translational* energy in promoting insertion, we measured the ratio of total reaction cross sections for stretch-excited methane (σ_s) to that for ground state methane (σ_g) accelerated to the same total energy. For each experiment σ can be calculated as the total signal level in the center-of-mass frame divided by the product of the number density of each reactant in the interaction volume and the relative velocity of the reactants.[21] Because our target is a ratio of cross sections, we use ratios of these parameters rather than absolute values. In this calculation we made each assumption or approximation conservatively, that is, in the direction that always produces a *strict lower limit* to the reactivity ratio (σ_s/σ_g). The ratio of center-of-mass signal levels was calculated during forward convolution fitting of the data. The ratio of Y beam number densities was measured by pulsed laser-induced fluorescence on the $^2P_{1/2} \leftarrow {}^2D_{3/2}$ line at 359.4 nm directly in the interaction region. The ratio of CH_4 number densities was taken to be the ratio of the CH_4 fractions in the gas mixtures. In the optical pumping experiment, the effective CH_4 (ν_3=1) number density is also proportional to the fraction of molecules pumped. This fraction is the product of three factors: the

fractional population of the lower state of the optical transition before interaction with the OPO, the fraction of this population excited by the OPO, and the fraction of the gas pulse illuminated by the OPO beam. Taking these factors into account (as described in *Experimental Methods*), we calculate that the total reactive cross section of the CH_4 antisymmetric stretch is ≥ 2.2 times the cross-section for ground-state CH_4.

Discussion

Our measured value of $\sigma_s/\sigma_g \geq 2.2$ represents a strict lower limit to the ratio of the total reaction cross-section for $Y + CH_4 \rightarrow YCH_2 + H_2$ at E_{coll} = 15.1 kcal/mol with one quantum of C-H antisymmetric stretching excitation (σ_s) to that at E_{coll} = 23.8 kcal/mol with no OPO irradiation (σ_g). In the OPO-off case, it is important to consider the role of vibrationally excited CH_4 molecules that may be present because of thermal excitation. It is known that vibrational energy is only cooled efficiently within vibrational levels of similar energies on supersonic expansion.[22] By using the CH_4 vibrational frequencies and degeneracies, at 300K ≈0.70% of the CH_4 molecules are vibrationally excited, with all but a negligible fraction in the low-energy excited bending levels v_4 (1306 cm^{-1}) and v_2 (1534 cm^{-1}). In experiments at 15.1 kcal/mol, it is unlikely that molecules containing vibrational energy because of thermal excitation (but are not pumped by the OPO) contribute significantly to the observed reactive signal. However, in the experiments at E_{coll} = 23.8 kcal/mol, a significant fraction of the observed signal could in principle result from reactions of bend-excited CH_4. To explore this possibility, experiments were carried out at the same collision energy using a nozzle heated to 380 K, where the population of bend-excited methane should be ≈ 4 times that at 300 K. No evidence for enhanced reactivity attributable to bend-excited methane was observed, strongly suggesting that the OPO-off signal is not dominated by reaction of bend-excited methane.

In reactions involving elimination of H or H_2, angular momentum conservation can play an important role in the dynamics. In particular, if complexes are produced with large total angular momenta, because of the small reduced mass of the products, centrifugal barriers in the exit channel can increase the fraction of complexes decomposing to reactants rather than to products.[23] The present experiments were carried out by pumping the v_3 Q(1) line of a jet-cooled sample of CH_4 molecules. In the reaction of vibrationally excited molecules, only one quantum of rotational angular momentum ($J = 1$) contributes to the total angular momentum of the $HYCH_3$ complexes. In reactions at high collision energy, although all J levels can contribute, because rotational cooling is expected to be nearly complete ($T < 5$ K), the contribution from higher rotational levels of methane will be negligible. Because of the large potential energy barrier to reaction, in particular for ground vibrational level molecules, reactions from small impact parameter (b) collisions will be dominant. Consequently, the maximum total angular momentum of complexes, which is primarily determined by the orbital angular momentum $L = \mu v b$, is highly restricted in both experiments. Therefore, the fraction of insertion complexes decaying to products should not differ significantly between the two experiments. Indeed, in studies of nonreactively scattered Y atoms at wide laboratory angles (corresponding to CM angles near 180^o) we were unable to observe any statistically significant difference in nonreactive scattering of Y atoms with the OPO on and off. Because of this, and because the barrier to insertion is the largest barrier on the PES, most $HYCH_3$ complexes decay to $YCH_2 + H_2$ rather than back to reactants.

The potential energy barriers for insertion of ground-state neutral transition metal atoms (having n valence electrons) into C-H bonds of hydrocarbon molecules result from the repulsive interactions between the ground state $d^{n-2}s^2$ or high-spin $d^{n-1}s^1$ electronic configurations of most neutral metal atoms and the directional sp^3

hybridized C-H σ-bond.[15,20] Successful reaction requires access to the low-spin $d^{n-1}s^1$ or d^ns^0 electronic configurations able to minimize long-range repulsive interactions and form the two new covalent bonds in the insertion complex. In the case of Y + CH_4, the adiabatic barrier for insertion results from the avoided crossings of diabatic curves associated with the repulsive doublet ground state $Y(d^1s^2) + CH_4$ and attractive doublet $Y(d^2s^1) + CH_4$ surfaces.

In gas-surface dissociative adsorption, gas phase abstraction reactions (e.g., Cl + CH_4), and in the insertion of a metal atom into a C-H bond, the initial antisymmetric normal mode excitation in the isolated methane molecule is delocalized over four C-H bonds. This energy must evolve into energy localized in the reaction coordinate during approach if reaction is to be successful. Theoretical calculations have allowed us to begin understanding the dynamics of these processes. In the case of dissociative methane adsorption, the symmetric stretch fundamental adiabatically correlates with localized excitation of the unique reacting C-H bond pointing toward the surface.[24,25] However, antisymmetric stretch excitation becomes localized away from the reactive bond in the spectator CH_3 moiety. Qualitatively similar behavior has been observed in theoretical studies of the gaseous abstraction reaction Cl + CH_3D.[26]

The subtle complexities underlying the relative efficacy for promoting polyatomic reactions by using different forms of energy are illustrated by the marked differences seen even in closely related systems. For example, Palma *et al.* have carried out theoretical analyses of reactions of ground state $O(^3P)$ atoms with vibrationally excited CH_4[27] and CH_3D.[28] For CH_4, large enhancement factors were predicted for both symmetric and antisymmetric stretching modes. However, in the deuterium-substituted case, although reactivity was enhanced substantially for symmetric stretching excitation, antisymmetric stretching was not very effective in promoting reaction. Similar subtle effects are evident in the gas-surface systems:

translational energy is more effective in promoting reaction of CH_4 than is an equivalent amount of energy in v_3 for Ni(100), whereas the situation is reversed for Ni(111). Recently, Bisson *et. al.* compared the dissociative adsorption of CH_4 ($2v_3$) on Pt(111) to that on Ni(111).[29] They found that excitation of CH_4 increases its reactivity by $>10^4$ on Ni(111), whereas the enhancement factor on Pt(111) is $\approx 10^2$. Although a fraction of this difference is attributable to the larger barrier height in the Ni reaction, it has been suggested that because of a longer C-H bond length at the transition state for Ni compared to Pt, reactant vibrational energy is better able to surmount the "later" barrier in the former case.

On the basis of the present results, one might be tempted to conclude by stating that, because the Y + CH_4 insertion reaction is enhanced more strongly by reactant vibrational energy than by an equivalent amount of translational energy, it represents a system involving a "late" potential energy barrier. In a vibrationally nonadiabatic model, reactant vibrational excitation provides access to lower-energy transition state geometries for reaction.[7] Although this explanation is appealing, the remarkable subtleties already identified in reactions involving a diverse range of polyatomic systems illustrate that simple concepts based on our understanding of three-atom reactions must be applied with great caution. In the absence of further experiments involving comparisons of other metals and other reactant vibrational modes, and because theoretical analysis remains to be done, generalizations on the basis of our study would be premature. Clearly, the combination of experiment and theory will be of tremendous value in unraveling the fundamental dynamics underlying how different forms of reactant energy promote this important class of chemical reactions.

Experimental Methods

The experimental apparatus employs a laser vaporization source to produce a beam containing ground-state Y atoms in neat H_2 or 20% H_2 in He.[30] The beam is

collimated by a 2-mm skimmer and a 1.7-mm x 1.7-mm square defining aperture, refined temporally by using a slotted chopper wheel, and crossed at right angles by a singly skimmed beam containing 5% or 10% CH_4 in H_2. For optical pumping experiments, the output of a pulsed narrow-band infrared optical parametric oscillator is arranged to cross the methane beam upstream of the collision region. After bimolecular reaction, some of the chemical products (YCH_2) drift ≈ 25 cm to a detector where they are photoionized by the output of an F_2 laser at 157 nm, pass through a quadrupole mass filter, and are detected by a dynode/electron multiplier combination. The rotatable source assembly makes it possible to rotate the two beams relative to the fixed detector. By measuring the time-of-arrival distributions of the products at the detector, the laboratory angular and kinetic energy distributions are determined for reaction or for nonreactive inelastic collisions.

The OPO is a home-built Nd:YAG-pumped unit based on the nonresonant oscillator and optical parametric amplifier stages of a known design.[31] The primary differences from that system are the use of a four crystal (two KTP, two KTA) amplifier stage and the replacement of the SLM OPO with a telecom distributed-feedback diode laser as the seed source.[32] The output is spectrally separated in a CaF_2 prism and tuned to the desired absorption resonance by using a photoacoustic cell while measuring the seed wavelength with a fiber-coupled wavemeter. The 3,018.8 cm^{-1} beam is aligned 5 mm upstream of the interaction region and softly focused to a spot <3 mm in diameter in the plane of the beams. The OPO bandwidth has been measured by linewidths in photoacoustic absorption spectra to be ≈ 1GHz. This is nearly 20 times the expected 41-MHz Doppler width of the ν_3 Q(1) transition transverse to the CH_4 beam calculated from the beam angular divergence; thus, the OPO covers the entire absorption feature. The sharp rise in product signal with the first 100 μJ of IR energy saturation curve in Figure 2.5 is consistent with the radiation

density provided by the OPO and the known oscillator strength of the transition. The much slower increase in signal at higher energies is characteristic of a beam profile containing a distribution of intensities and the trendline in Figure 2.5 has been calculated by using such a distribution. This is consistent with the non-uniform beam profile observed with this OPO and typical of this design.

Determination of the fraction of the CH_4 beam pumped by the OPO is as follows. The hydrogen nuclear spin statistics in methane are such that each of the nuclear modifications has a different lowest allowed J state: J = 0, 2, and 1 for the A, E, and F modifications, respectively.[33] Modifications do not exchange on the microsecond timescale of a supersonic expansion, so in the limit of complete rotational cooling the populations of each of these J states in the beam are identically the populations of the modifications at room temperature thermal equilibrium: 5/16, 2/16, and 9/16 for A (J = 0), E (J = 2), and F (J = 1), respectively.[34] We pumped the Q(1) line of ν_3, so the lower state is J = 1 and the maximum fractional population is 9/16. The OPO saturated the transition, so the excitation fraction is given by the ratio of the upper-state statistical weight to the sum of the upper- and lower- state statistical weights.[35] Both states have an extra threefold degeneracy from the F modification in addition the normal ($2J$ + 1) rotational degeneracy for a total of nine, as tabulated in the HITRAN database.[36] The saturated fractional excitation is thus 1/2. The fraction of the gas pulse that was illuminated was calculated geometrically. The Y beam was mechanically chopped by a slotted disc of 10.9-cm radius with a 1-mm-wide slit spinning at 210 Hz providing a shutter function ≈ 7.0 μs wide. The methane (10% in H_2) beam has a mean velocity of 2,123 m/s, so a 7.0 μs pulse is 14.9 mm long. The 3.0-mm spot size of the OPO in the plane of the beams thus illuminates 20% of the beam. The fraction of the methane flux in the ν_3 state is therefore (9/16)(1/2)(0.20) = 5.6%.

Acknowledgements

This research was supported by the National Science Foundation Grant CHE-0316296.

REFERENCES

[1] Polanyi, J. C. *Science* **1987**, *236*, 680.

[2] Crim, F. F. *Accounts of Chemical Research* 1999, *32*, 877.

[3] Zare, R. N. *Science* **1998**, *279*, 1875.

[4] Yan, S.; Wu, Y.-T.; Zhang, B.; Yue, X.-F.; Liu, K. *Science* **2007**, *316*, 1723.

[5] Crim, F. F. *Science* **2007**, *316*, 1707.

[6] Juurlink, L. B. F.; McCabe, P. R.; Smith, R. R.; DiCologero, C. L.; Utz, A. L. *Physical Review Letters* **1999**, *83*, 868.

[7] Smith, R. R.; Killelea, D. R.; DelSesto, D. F.; Utz, A. L. *Science* **2004**, *304*, 992.

[8] Higgins, J.; Conjusteau, A.; Scoles, G.; Bernasek, S. L. *Journal of Chemical Physics* **2001**, *114*, 5277.

[9] Juurlink, L. B. F.; Smith, R. R.; Killelea, D. R.; Utz, A. L. *Physical Review Letters* **2005,** *94*, 208303.

[10] Maroni, P.; Papageorgopoulos, D. C.; Sacchi, M.; Dang, T. T.; Beck, R. D.; Rizzo, T. R. *Physical Review Letters* **2005**, *94*, 246104.

[11] Lersch, M.; Tilset, M. *Chemical Reviews* **2005**, *105*, 2471.

[12] Godula, K.; Sames, D. *Science* **2006**, *312*, 67.

[13] Niu, S.; Hall, M. B. *Chemical Reviews* **2000**, *100*, 353.

[14] Wittborn, A. M. C.;, Costas, M.;, Blomberg, M. R. A.; Siegbahn, P. E. M. *Journal of Chemical Physics* **1997**, *107*, 4318.

[15] Carroll, J. J.; Haug, K. L.; Weisshaar, J. C.; Blomberg, M. R. A.; Siegbahn, P. E. M.; Svensson, M. *Journal of Physical Chemistry* **1995**, *99*, 13955.

[16] Henkelman, G.; Jonsson, H. *Physical Review Letters* **2001**, *86*, 664.

[17] Nave, S.; Jackson, B. *Physical Review Letters* **2007**, *98*, 173003.

[18] Stauffer, H. U.; Hinrichs, R. Z.; Schroden, J. J.; Davis, H. F. *Journal of Physical Chemistry A* **2000**, *104*, 1107.

[19] Li, T.; Cheng, W.; Liu, J.; Xie, X.; Cao, H. *Journal of Molecuar Structure: Theochem* **2006**, *761*, 83.

[20] Blomberg, M. R. A.; Siegbahn, P. E. M.; Svensson, M. *Journal of the American Chemical Society* **1992**, *114*, 6095.

[21] Lee, Y. T. In *Atomic and Molecular Beam Methods, volume I*; Scoles, G., Ed.; Oxford University Press, New York, 1988; pp 553-568.

[22] Bronnikov, D. K.; Kalinin, D. V.; Rusanov, V. D.; Filimonov, YU. G.; Selivanov, YU. G.; Hilico, J. C. *Journal of Quantitative Spectroscopy and Radiative Transfer* **1998**, *60*, 1053.

[23] Willis, P. A.; Stauffer, H. U.; Hinrichs, R. Z.; Davis, H. F. *Journal of Physical Chemistry A* **1999**, *103*, 3706.

[24] Halonen, L.; Bernasek, S. L.; Nesbitt, D. J.; *Journal of Chemical Physics* **2001**, *115*, 5611.

[25] Milot, R.; Jansen, A. P. J. *Physical Review B* **2000**, *61*, 15657.

[26] Yoon, S.; Holiday, R. J.; Sibert, E. L. III; Crim, F. F. *Journal of Chemical Physics* **2003**, *119*, 9568.

[27] Palma, P.; Clary, D. C. *Physical Chemistry Chemical Physics* **2000**, *2*, 4105.

[28] Palma, P.; Echave, J.; Clary, D. C. *Chemical Physics Letters* **2002**, *363*, 529.

[29] Bisson, R.; Sacchi, M.; Dang, T. T.; Yoder, B.; Maroni, P.; Beck, R. D. *Journal of Physical Chemistry A* **2007**, *111*, 12679.

[30] Willis, P. A.; Stauffer, H. U.; Hinrichs, R. Z.; Davis, H. F. *Review of Scientific Instruments* **1999**, *70*, 2606.

[31] Bosenberg, W. R.; Guyer, D. R. *Journal of the Optical Society of America B* **1993**, *10*, 1716.

[32] Kulatilaka, W. D.; Anderson, T. N.; Bougher, T. L.; Lucht, R. P. *Applied Physics B* **2005**, *80*, 669.

[33] Herzberg, G. *Molecular Spectra and Molecular Structure II. Infrared and Raman Spectra of Polyatomic Molecules*; D. Van Nostrand: Princeton, 1945; pp 37-42.

[34] Hepp, M.; Winnewisser, G.; Yamada, K. M. T. *Journal of Molecular Spectroscopy* **1994**, *164*, 311.

[35] Bernstein, R. B. *Chemical Dynamics via Molecular Beam and Laser Techniques*; Oxford University Press: New York 1982; pp 38-44.

[36] Rothman; Jacquemart, D.; Barbe, A.; Chris Benner, D.; Birk, M.; Brown, L. R.; Carleer, M. R; Chackerian Jr., C.; Chance, K.; Coudert, L. H.; Dana, V.; Devi, V. M.; Flaud, J.-M.; Gamache, R. R.; Goldman, A.; Hartmann, J.-M; Jucks; Maki, A. G.;

Mandin, J.-Y.; Massie, S. T.; Orphal, J.; Perrin, A.; Rinsland, C. P.; Smith, M. A. H.; Tennyson, J.; Tolchenov, R. N.; Toth, R. A.; Vander Auwera, J.; Varanasi, P.; Wagner, G. *Journal of Quantitative Spectroscopy and Radiative Transfer* **2005** *96*, 139.

CHAPTER 3

IMPROVED PIEZOELECTRIC ACTUATORS FOR USE IN HIGH-SPEED PULSED VALVES

Introduction

Pulsed molecular beams are generated by supersonic expansion from a high-pressure gas reservoir to a low-pressure vacuum chamber through an orifice opened briefly by a high-speed pulsed valve. These beams are routinely used in those scattering and spectroscopy experiments where the low duty cycle of the gas load makes the most efficient use of available pumping speed and the molecular pulse repetition rate can be matched to the rate of pulsed lasers being used in beam generation or detection. The primary difference in equipment between a pulsed and a continuous beam source is the pulsed valve, for which many designs have been proposed and several are now widely accepted. One design that is in widespread use is the piezoelectrically actuated valve of Proch and Trickl.[1] It has many characteristics of the ideal pulsed valve: repetition rates up to 1 kHz, no upper limit to the pulse length, orifice sizes up to 1 mm, a simple power supply, and long-term stability and reliability. The most prominent shortfalls of this valve are its minimum pulse length—around 250 μs for a 1-mm nozzle—and the limited chemical resistance of its actuator. Proch and Trickl's design for the valve uses a commercially available piezoelectric disc bimorph actuator manufactured by Physik Instrumente (PI) for motion transduction. By using this "off the shelf" actuator, the user needs only to undertake in-house fabrication of a few relatively simple mechanical parts to obtain a working valve.

Despite the convenience of this commercially available actuator, we recently undertook a project aimed at assembling our own actuators. We did this with three goals in mind: 1) to have actuators available with a shorter lead time and lower cost than the PI part, 2) to find an insulating coating for the piezo crystal more chemically inert than the polymer used by PI, and 3) to explore actuator designs that might produce shorter pulses. As PI has recently ceased production of the actuator around which the Proch-Trickl valve was designed, this project has taken on a more urgent purpose: our materials and methods will enable laboratories satisfied with these valves to continue producing and using them.

Actuator Designs and Construction

The PI P-286.23 disc translator originally used by Proch and Trickl is a piezoelectric bimorph consisting of a 0.5 mm thick stainless steel annular shim (41 mm OD, 10 mm ID) concentrically glued to a 0.5 mm thick annulus of PZT piezoelectric ceramic (38 mm OD, 13 mm ID). The shim is sandwiched on its outer edge by a pair of stainless steel rings which provide a bolt circle for mounting the actuator to the valve. One electrical lead is soldered to the "front" surface of the piezo and another to the inner surface of one of the mounting rings. This ring is in electrical contact with the steel shim and hence the "back" side of the piezo crystal. The valve is opened by applying a negative high voltage pulse to the "front" lead attached to the piezo while the "back" lead is held at ground (Figure 3.1a). The applied voltage induces a radial contraction of the piezo crystal and hence a radial shear between the crystal and shim, causing the assembly to cup. A plunger, attached to the actuator through the center hole via a pair of special nuts, carries an o-ring at its tip to seal the orifice between pulses.

We constructed actuators with shims and piezo crystals of the same dimensions as those in the PI part to allow reuse of the PI mounting rings and other valve parts

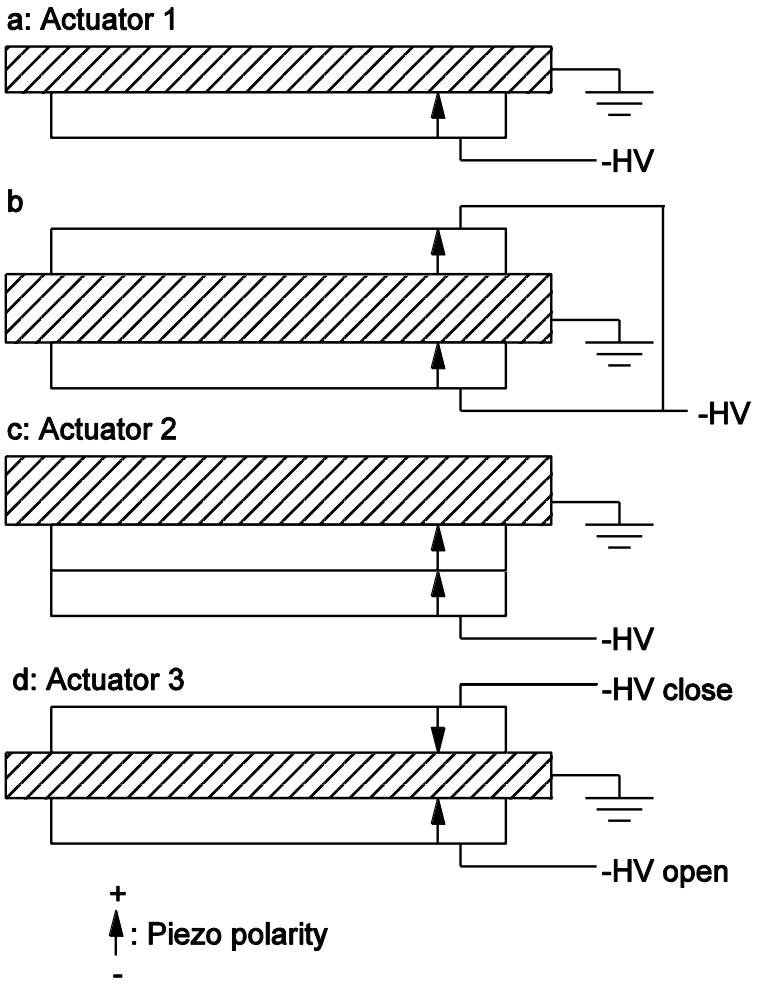

Figure 3.1: Actuator designs. Hashed region is the stainless steel shim. The nozzle orifice is towards the bottom of the page and the valve opens when the center of the actuator bows up.

already on hand. The shims were fabricated from 304 stainless steel shim stock using standard machining techniques and the piezo crystals were obtained from PI (part PTYY-0153) with fired silver electrodes on both faces, the polarity being marked on the positive face. We first constructed a near-replica of the PI P-286.23 to ensure that our actuators would have, at a minimum, the same performance to which we were accustomed. A shim and piezo were first cleaned with anhydrous methanol and allowed to dry. Then the positive face of the piezo was glued to the shim using a thin

layer of solvent-free, silver-filled epoxy (Resinlab SEC1233) to ensure electrical contact. The epoxy was also used to attach a PTFE-insulated lead to the exposed negative face of the piezo. We found this to be more reliable than soldering the lead, which risks overheating the piezo. After allowing the epoxy to cure for 24 hours, the assembly was again cleaned with anhydrous methanol and the exposed negative face of the piezo was coated by hand with an automotive paint designed for rust prevention (Magnet Paints Chassis Saver) and has withstood submersion in acids and halogenated hydrocarbons in our testing. The paint was mixed by stirring rather than shaking to avoid formation of bubbles in the finish. After curing overnight, the actuator was installed in a valve and found to perform indistinguishably from the commercial PI part.

Having accomplished the goals of replicating the commercial actuator and enhancing its resistance to chemical attack, we explored alternate configurations hoping to achieve shorter minimum pulse durations. Our first idea was to use a thicker, stiffer shim to increase the resonance frequency and hence the restoring force that closes the valve. A single piezo could be driven at a higher voltage to provide more opening force. Such an actuator was constructed with a 0.71 mm thick shim, but its performance was roughly equivalent to a normal actuator. This was because the capacitance of the piezo limits the voltage rise time such that the longer pulse duration required to achieve a higher opening voltage also extended the duration of opening beyond the natural resonance time of the actuator. To increase the opening force of the actuator without requiring higher voltages, we constructed a dual-actuator design using a stainless steel shim 0.71 mm thick with one piezo crystal glued to each side. One crystal was oriented with its positive face exposed, one with its negative face exposed (Figure 3.1b). A lead was glued to each piezo allowing application of the same negative high voltage pulse to both piezos. In this arrangement the “front” piezo

is arranged as in the PI part, but the additional "back" piezo is expanded rather than contracted because the applied voltage is opposed to its internal polarity. This design was found to provide shorter opening times than the PI part, but two shortcomings convinced us to continue investigating other designs. First, the total applied voltage had to be limited to -500 V to avoid depolarizing the back piezo, as the voltage applied to it is opposed to its internal polarity. Second, the voltage rise time was significantly longer than for the single piezo actuator, limiting the minimum electrical pulse duration to 160 μs to achieve -500 V. This is due to the increased capacitance from placing the two piezos electrically in parallel. To overcome these limitations, we pursued another design.

In this second dual-piezo design, we used the thicker shim but placed two piezo crystals electrically in series by gluing the second piezo directly to the first one, forming a stack to which a single high voltage lead attached to the exposed negative face of the top piezo could charge both crystals, with each seeing half of the total voltage (Figure 3.1c). By placing the piezos in series the equivalent circuit capacitance is lowered and the overall voltage rise time becomes much shorter. A small construction note: the two piezos are thick enough that the top surface of the stack will interfere with the ground lead solder joint on the PI mounting ring. This lead is redundant if the actuator is affixed to the grounded valve body with conductive screws, so we removed it.

We also constructed a dual-piezo actuator based on a different design principle altogether. Rather than using a stiffer shim to passively close the valve faster, we used a labile shim in conjunction with a second piezo configured to drive the valve closed when energized by a separate voltage pulse. To accomplish this, a piezo was glued to each side of a 0.5 mm thick shim with the negative faces of both crystals exposed

(Figure 3.1d). A valve body was modified to include a second electrical feedthrough so each piezo could be supplied with a separately timed voltage pulse.

Results

The newly-built actuators were installed in a 1 mm orifice valve and tested in the Cornell Rotatable Source Crossed Molecular Beams Machine[2]. Comparative data is shown for the single piezo actuator (Actuator 1, Figure 3.1a), the series dual-piezo actuator (Actuator 2, Figure 3.1c) and the actively closed actuator (Actuator 3, Figure 3.1d). The exposed faces of the piezos in all the actuators were coated with Chassis Saver. The valve, energized by a square negative high voltage pulse of adjustable height and duration provided by a home-built pulser (or two, for Actuator 3), was mounted in a source differential region pumped by two 6 inch diffusion pumps. The beam passed through a skimmer (2 mm orifice) into a second differentially pumped region, then through a defining aperture (3 mm square) into the main chamber evacuated by a 2000 l/s turbomolecular pump. Here the beam could be chopped by a high-speed mechanical chopper wheel (two 1 mm wide slots, 10.9 cm radius, 210 Hz rotational speed) transmitting a segment of the pulse approximately 8 μs long. The rotatable source assembly was set to point the beam directly at the 200 μm diameter input aperture of the detector, a triply differentially pumped quadrupole mass spectrometer using 100 eV electron impact ionization, -4 kV conversion dynode, and a continuous electron multiplier operating in the pulse counting mode. The output signal of the multiplier was fed to a multichannel scaler (SRS SR430). A digital delay generator (BNC 555) provided 30 Hz triggers to the pulser(s) and scaler. The delay generator and scaler settings were controlled through a GPIB interface to a PC via a custom LabView data acquisition program.

Helium (Airgas UHP grade) was used to test the new actuators at 5 psig and 60 psig backing pressures. The intensity of the beam as a function of time was measured

by setting the quadrupole to transmit M/z = 4 and measuring the time of arrival distribution with the scaler (bin width = 5.12 μs) without chopping the beam. Optimum high voltage pulse settings for each actuator were found to be 60 μs at -500 V for Actuator 1 at both backing pressures, 120 μs at -760 V for Actuator 2 at 5 psig and 60 μs at -760 V for 60 psig, and 60 μs at -550 V to open/60 μs at -550 V with a 60 μs delay to close for Actuator 3 at both backing pressures. These settings provided the largest signal at the peak of the distribution for each actuator. Longer pulses and higher voltages were not found to increase the peak beam intensity, but did increase the average pressure in the source region as measured with a Bayard-Alpert ionization gauge. Under optimal pulse conditions the source pressure during operation of Actuators 2 and 3 was approximately half that measured during operation of Actuator 1. Peak intensity was used as the optimization criterion for the adjustment of pulse conditions, rather than peak intensity while avoiding secondary pulses caused by bouncing of the seal upon closing. Proch-Trickl valves produce pulses too long to provide good time-of-flight resolution on their own, so beams produced by these valves must be mechanically chopped if such resolution is required, in which case the valve's firing can be timed such that the peak intensity is directed through the chopper and small secondary pulses cause no detriment to the experiment except to slightly increase the gas load in the source region. The beam intensity profiles are shown in Figure 3.2.

We investigated possible distortion of the profiles arising from inconstant beam velocity during the pulse by mechanically chopping the beam at several points in a 150-μs range within the pulse and measuring the resulting time-of-flight distributions. The width of the velocity distribution did not measurably change within the pulse, but the peak velocity was found to change by approximately 10%, being fastest at the beginning of the pulse and slowest in the late tail. This 10% change in

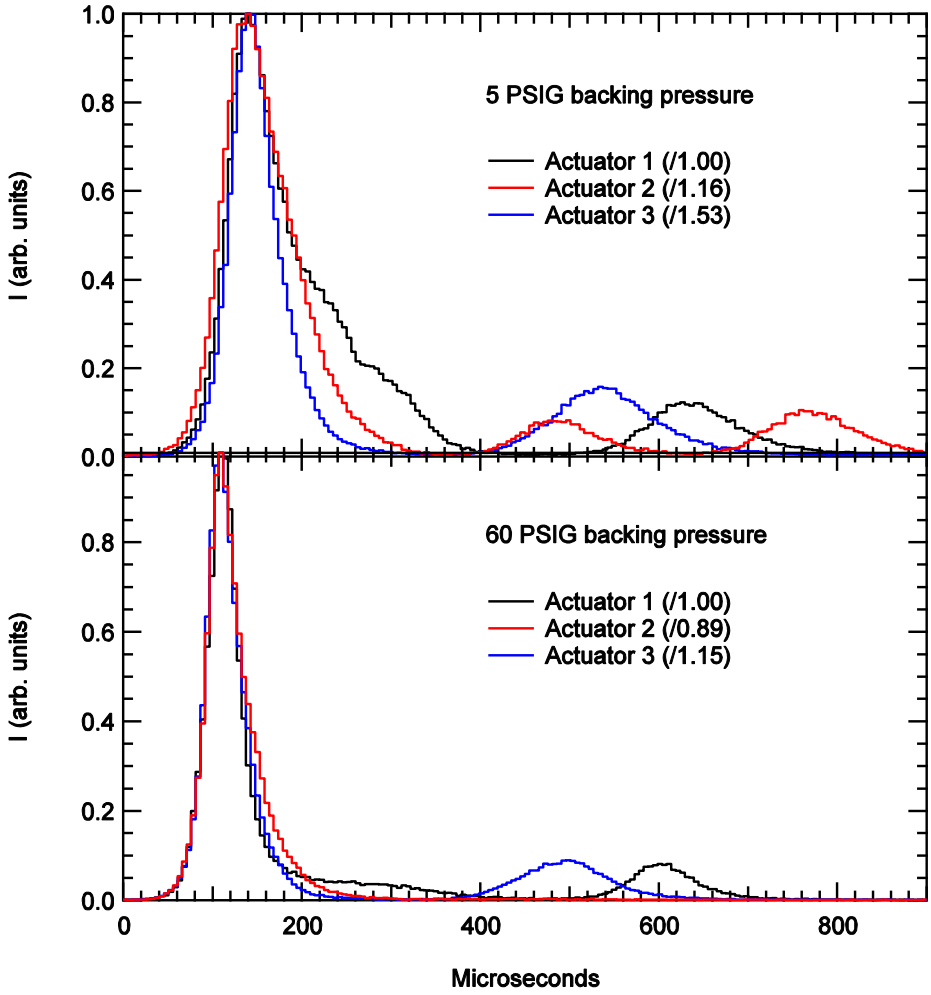

Figure 3.2: Helium beam intensity profiles from three different actuator designs.

peak velocity could, at most, cause approximately 20 μs of broadening of the unchopped distributions over the 150 μs range in which it was measured. Because of this effect it should be kept in mind that the distributions in Figure 3.2 represent an upper limit on the width of the pulses as they would appear closer to the valve. Although this measurement procedure involves passage through a skimmer and a relatively long flight distance (~33 cm from nozzle to detector) rather than probing the gas pulse directly in front of the nozzle as is typical when using a fast ion gauge[3], it does examine as a unit the valve/skimmer system commonly used to produce a

supersonic molecular beam. This data therefore represents gas pulses actually delivered to the interaction region of a typical scattering experiment.

Under the conditions of greatest peak intensity, all the actuators exhibited a secondary pulse from the seal bouncing upon closing. Actuator 2 opened the valve much earlier than the other actuators relative to the voltage pulse, by 30 μs at 5 psig and 25 μs at 60 psig. The profiles for all the actuators are shown in Figure 3.2 normalized to the peak intensity of Actuator 1, the single-piezo design, and translated such that the peak intensities coincide to allow easy comparisons between the widths and shapes of the profiles. The normalization constants are also given in Figure 3.2 and show that with a 5 psig backing pressure Actuators 2 and 3 both provide greater beam intensity than Actuator 1. With a 60 psig backing pressure Actuator 2 shows a decrease in peak intensity, but Actuator 3 shows an increase. The widths of the profiles are strongly influenced by the gas-dynamic shutter effect[4,5] from the leading edge of the pulse reflecting from the chamber wall and attenuating the latter part of the pulse while forming a pressure shock. This effect makes all the profiles exhibit peak intensity at the leading edge of the pulse. The 5 psig profiles display less of this effect than the 60 psig traces due to the smaller gas densities involved. Because of this the 5 psig profiles most clearly demonstrate the shorter opening time of the new actuators: the full-width at half-maximum of the profiles are 72 μs for Actuator 1, 87 μs for Actuator 2, and 61 μs for Actuator 3. The higher gas load when using Actuator 1 provides a stronger shutter effect compared to the new actuators, making its full-width at half-maximum lower than would be expected. The relatively high intensity tail of the profile for this actuator, extending for about 100 μs longer than for either of the other profiles is evidence of its longer opening duration. The shutter effect is strong enough at 60 psig that all the actuators deliver the same FWHM of 46 μs. The profiles differ only in the late, low intensity tail of the pulse. For Actuator 1 this tail still

extends about 100 μs longer than for the new designs. The late tail is slightly less intense for Actuator 3 than for Actuator 2 while the peak intensity is greater.

Discussion

These profiles demonstrate that for pressures between 5 and 60 psig Actuator 3 provides the greatest peak intensity and the lowest gas consumption of the actuators tested. This comes at the cost of added complexity, requiring two independent high voltage pulses to actuate the valve. Actuator 2, however, also provides universally shorter pulses than Actuator 1 with approximately the same gas consumption as Actuator 3. Its only drawback compared to Actuator 1 is a decrease in peak intensity of about 10% when used with high backing pressures. This would be the most appropriate actuator in the case of an experiment where low gas consumption was required (i.e. an expensive reagent) and a second high voltage pulse is not available to allow the use of Actuator 3.

It is interesting to note that at 5 psig, we investigated the effect of only changing the pulse duration, while all other parameters were held constant. This was done by operating Actuator 3 with and without the "close" pulse. When the "close" pulse on Actuator 3 was disabled, causing it to behave essentially like Actuator 1, not only did the profile become wider and the source pressure increase, both to levels similar to that of Actuator 1, but the peak intensity also decreased by approximately 15%. This lower intensity under identical opening forces and backing pressures but different closing forces is especially clear evidence that, in the case of a skimmed beam from a valve with a relatively long opening duration, the gas dynamic shutter effect is a strong limiter of the peak beam intensity. Decreasing the pulse duration without increasing the backing pressure will not only reduce gas consumption under these conditions but will increase the peak beam intensity. It was also found that a 400 μs, -400 V "close" pulse strongly suppressed bounces in Actuator 3.

Unfortunately this coincides with an increase of the primary pulse duration. The higher "close" pulse voltage seems to be required to quickly close the valve, so perhaps a more complex "close" pulse with a short duration of higher voltage to close the valve, followed by a drop to a lower voltage maintained for a longer duration to keep the valve closed would be ideal.

To summarize, we present materials and methods for the assembly of actuators suitable for use in Proch-Trickl pulsed gas valves. These actuators have performance equal to and resistance to chemical attack superior the recently discontinued commercial actuator around which the valve was originally designed. Additionally, we present new actuator designs that open the valve for shorter durations than the original actuator, resulting in reduced gas consumption and lower average source chamber pressures for a given backing pressure and pulse rate.

Acknowledgements

We wish to thank Prof. Timothy Minton for enlightening discussions regarding his own modifications to the Proch-Trickl design. This research was supported by the National Science Foundation Grant CHE-0316296 and the United States Department of Energy Grant DE-FG02-00ER1505095.

REFERENCES

[1] Proch, D.; Trickl, T. *Review of Scientific Instruments* **1989**, *60*, 713.

[2] Willis, P. A.; Hinrichs, R. Z. ; Stauffer, H. U.; Davis, H. F. *Review of Scientific Instruments* **1999**,*70*, 2606.

[3] Gentry, W. R.; Giese, C. F. *Review of Scientific instruments* **1978**, ***49***, 595.

[4] Bassi, D.; Iannotta, S.; Niccolini, S. *Review of Scientific Instruments* **1981**, *52*, 8.

[5] Makarov, G. N. *Chemical Physics Letters* **2002**, *358*, 307.